Int. J. Electrochem. Sci., 6 **(2011)** 1342 - 1354

International Journal of ELECTROCHEMICAL SCIENCE
www.electrochemsci.org

Electrochemistry and Impedance Studies on Titanium and Magnesium Alloys in Ringer's Solution

A.M. Fekry[*] *and M.A. Ameer*

Chemistry Department, Faculty of Science, Cairo University, Giza-12613, Egypt.
[*]E-mail: hham4@hotmail.com

Received: 3 March 2011 / *Accepted:* 29 March 2011 / *Published:* 1 May 2011

A study of both electrochemical behavior and hydrogen evolution reaction for both Ti–6Al–4V and AZ31E alloys are evaluated in Ringer's solution (RS) at 37 °C using different electrochemical techniques and scanning electron microscope (SEM) technique. Electrochemical measurements involve electrochemical impedance spectroscopy (EIS) tests by comparing the measured resistance variation with immersion time for both alloys. Also, potentiodynamic polarization technique used to evaluate the corrosion current density and hydrogen evolution for both alloys and comparing them. Impedance measurements show high corrosion resistance for the film formed on titanium alloy than that formed on magnesium alloy in RS solution at 37 °C, indicating a highly stable film. The low value of current density or hydrogen evolution for titanium alloy to that of magnesium alloy indicates the passivity of the former in the studied medium.

Keywords: Ti-alloy, Mg-alloy, EIS, SEM, ringer's solution (RS).

1. INTRODUCTION

The study of innovative biodegradable implant materials is one of the most interesting research topics in the area of biomaterials. Titanium alloys are used in implantology for their high corrosion and mechanical resistance in biofluids [1]. The behavior of these alloys is usually a combination of the electrochemical, hydrogen evolution, physiological and mechanical effects. Electrochemically, titanium alloys have high resistance as a result of their very stable oxide films formed by titanium dioxide (TiO_2), which is the most stable oxide of titanium, and some suboxides. All papers confirmed the predominant presence of TiO_2 with small quantities of suboxides TiO and Ti_2O_3. For Ti–6Al–4V alloy, the inner metal-oxide interface contains TiO_2, TiO and Ti_2O_3 while the outer oxide-solution interface is enriched with Al_2O_3. The physiological and electrochemical properties of titanium dioxide

film and its long-term stability in biofluids play an important role for the biocompatibility of titanium and its implant alloys. Titanium alloys are among the most used metallic biomaterials, particularly for orthopedic applications [2], they possess a set of suitable properties such as low specific weight, high corrosion resistance and biocompatibility. Titanium alloys form a thin, protective oxide film on their surface and are widely used as implant materials for failed hard tissues because of their good compatibility with bone.

On the other side, magnesium is an exceptionally light weight metal with a density of 1.74 g/cm^3 which is 1.6 and 4.5 times less dense than aluminum and steel, respectively. The fracture toughness of magnesium is greater than that of ceramic biomaterials such as hydroxyapatite, while the elastic modulus and compressive yield strength of magnesium are closer to those of natural bone [3]. Moreover, magnesium is essential to human metabolism and is naturally found in bone tissue [2, 3]. It is the fourth most abundant cation in the human body, with an estimated 1 mol of magnesium stored in the body of a normal 70 kg adult, with approximately half of the total physiological magnesium stored in bone tissue [3]. Biodegradable implant materials in the human body can be gradually dissolved, absorbed, consumed or excreted, so there is no need for the secondary surgery to remove implants after the surgery regions have healed. Metallic materials continue to play an essential role as biomaterials to assist with the repair or replacement of bone tissue that has become diseased or damaged. Thus, it is projected that magnesium and its alloys can be applied as lightweight, degradable, load bearing orthopedic implants, which would remain present in the body and maintain mechanical integrity over a time scale of 12–18 weeks while the bone tissue heals, eventually being replaced by natural tissue [3].

This work reviews the biological performance of Ti–6Al–4V and AZ31E alloys with immersion time at 37 ^oC in Ringer's solution that have been used as orthopedic biomaterials. The study is furthermore aimed to know the nature of the corrosion films formed and hydrogen evolution by comparing the behavior of Ti–6Al–4V and AZ31E alloys using conventional electrochemical techniques complemented with surface examination. Also, it is aimed to point out the attention for using magnesium alloys instead of titanium alloys in human body.

2. EXPERIMENTAL

Ti-6Al-4V alloy supplied from Johnson and Matthey (England) with composition (wt%); 5.7 Al, 3.85 V, 0.18 Fe, 0.038 C, 0.106 O and 0.035 N and the balance titanium. An extruded magnesium aluminum alloy (AZ31E) was donated from Department of mining, Metallurgy and Materials Engineering, Laval University, Canada with composition (wt%): 2.8 Al, 0.96 Zn, 0.28 Mn, 0.0017 Cu, 0.0111 Fe, 0.0007 Ni, 0.0001 Be and the balance Mg. The two alloys were tested in the present study. A coupon of the alloy was welded to an electrical wire and fixed with Araldite epoxy resin in a glass tube leaving a cross-sectional area of the specimen 0.196 cm^2 for both AZ31E and Ti-6Al-4V alloys. Ringer's solution [1] (g/L); NaCl (8.6); $CaCl_2$ (0.33); KCl (0.3), with a high concentration of NaCl was used to study the resistance of these alloys in a very aggressive biofluid. All reagents were Analar and RS solution was prepared using triply distilled water. The surface of the test electrode was mechanically polished by emery papers with 400 up to 1000 grit to ensure the same surface roughness,

degreasing in acetone, rinsing with ethanol and drying in air. The cell used was a typical three-electrode one fitted with a large platinum sheet of size 15 x 20 x 2 mm as a counter electrode (CE), saturated calomel (SCE) as a reference electrode (RE) and the alloy as the working electrode (WE). The impedance diagrams were recorded at the free immersion potential (OCP) by applying a 10 mV sinusoidal potential through a frequency domain from 10 kHz down to 100 mHz. Cathodic and anodic polarization curves were scanned from -2.0 V to 1.0 V for AZ31E alloy and from -1.0 V to 1.0 V for Ti-alloy with a scan rate of 1 mV s^{-1}.The instrument used was the electrochemical workstation IM6e Zahner-elektrik, GmbH, (Kronach, Germany). The SEM micrographs were obtained using a JEOL JXA-840A electron probe microanalyzer. The electrochemical measurements were always carried inside an air thermostat which was kept at 37 ^{o}C, unless otherwise stated. All potentials were measured and given with respect to saturated calomel electrode (SCE) (E = 0.241 V/SHE).

3. RESULTS AND DISCUSSION

3.1. Electrochemical impedance

Impedance measurements for Ti-Al-4V alloy in RS solution are presented as Bode plots in Fig. 1(a-c). Highly capacitive behavior is observed from medium to low frequencies, as indicated by phase angles approaching 90◦, suggesting that a highly stable passive film is formed on titanium alloy in Ringer's solution.

Table 1. Impedance parameters of Ti-6Al-4V alloy in RS at 37 ^{o}C.

Time	R_s /	R_p /	Q_p /	R_b /	Q_b /	α
Hour	Ω cm^2	Ω cm^2	μF cm^{-2}	MΩ cm^2	μF cm^{-2}	
0.00	7.03	4.31	23.0	0.02	15.1	0.87
0.50	6.58	4.35	22.4	0.92	14.9	0.87
1.00	6.41	4.72	22.3	1.13	13.6	0.87
2.00	6.14	5.01	22.3	1.19	12.6	0.88
4.00	6.03	5.32	22.1	1.23	12.5	0.88
8.00	5.64	5.99	21.3	3.35	11.5	0.88
12.00	5.63	6.03	18.9	5.74	9.92	0.89
16.00	4.87	6.09	12.3	10.9	4.91	0.87
20.00	4.91	6.37	9.41	13.2	4.74	0.87
30.00	4.21	6.89	9.34	17.4	4.53	0.88
45.00	3.98	7.05	7.74	21.6	4.11	0.89
70.00	3.98	7.18	6.53	26.2	3.97	0.89
100.00	3.69	7.91	6.37	34.2	3.86	0.89

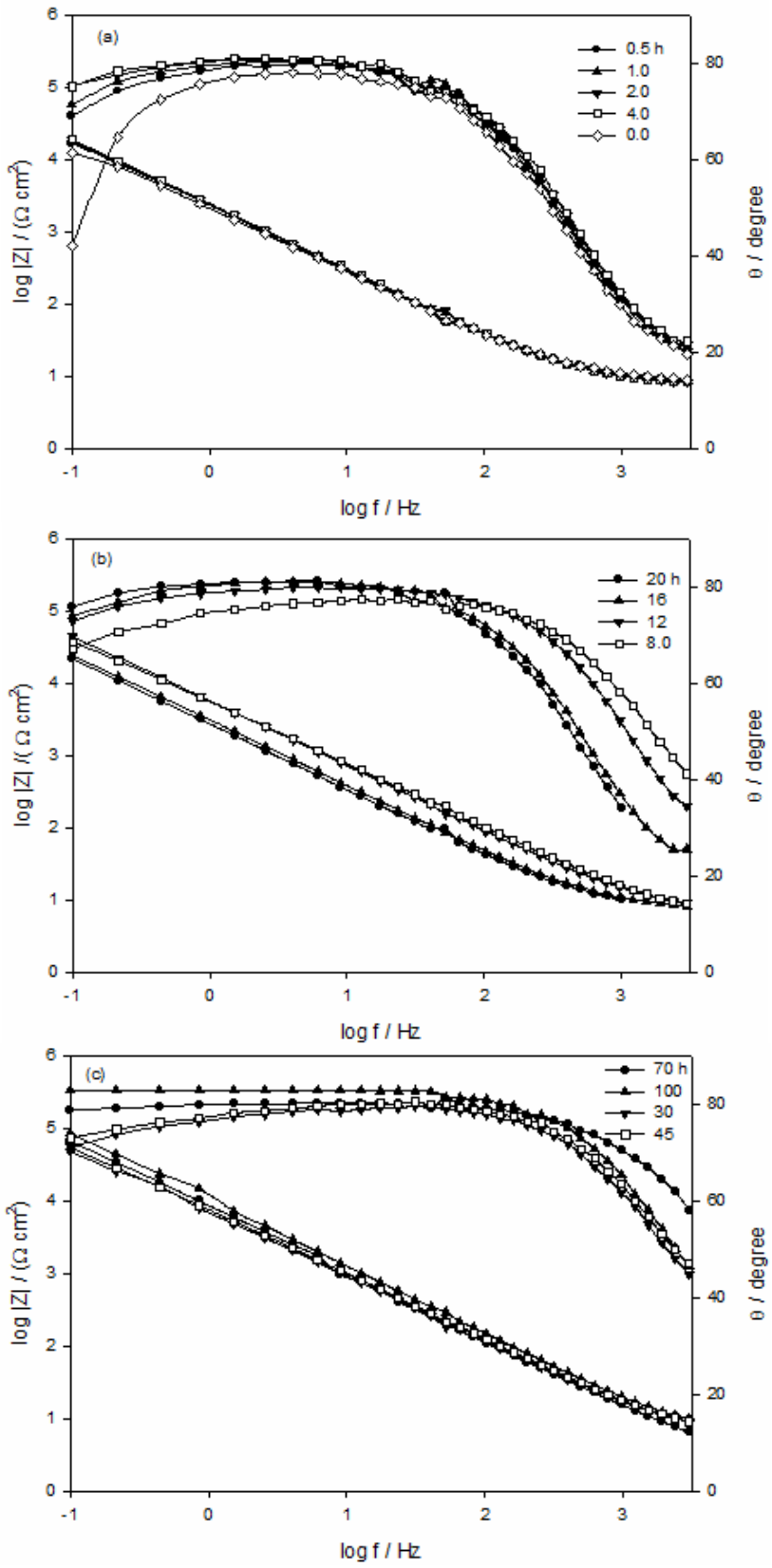

Figure 1 (a-c). Bode plots of Ti-6Al-4V alloy as a function of immersion time in RS at 37 ^{o}C.

The phase peak becomes broader by increasing immersion time till 100 h, with increasing phase angle maximum θ_{max}. It is of inertest to note that an increase in immersion time, from 0 to 4.0 h (Fig. 1a), causes a limited increase in |Z| and θ_{max} values, whereas from 8.0 to 20 h (Fig. 1b), impedance and θ_{max} values increase gradually. For longer immersion times, from 30-70 h (Fig. 3c), a more pronounced increase in either |Z| or θ_{max} value is observed with increase in immersion time.

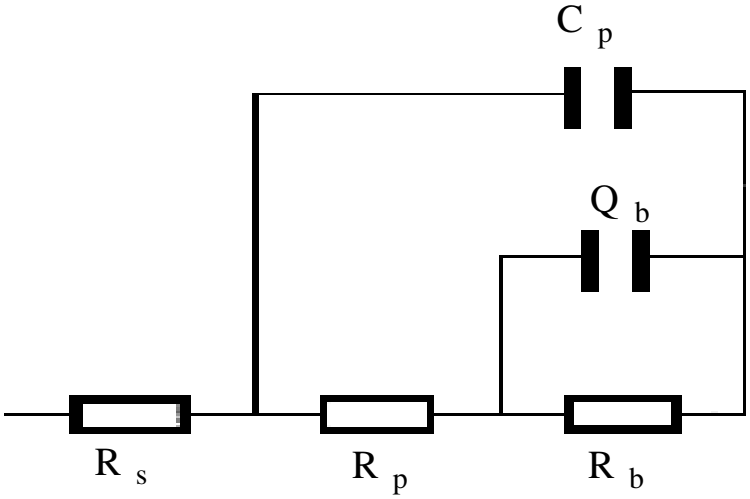

Figure 2. Equivalent circuit model representing two parallel time constants for an electrode/electrolyte solution interface.

The large broad phase angle peak indicates an interaction of two time constants. According to the literature [4, 5] the film on Ti alloys is composed of a bi-layered oxide consisting of a porous outer layer and a barrier inner layer [2]. The data was analyzed using the two parallel time constants model shown in Fig. 2 which best fits the data and was always proposed for porous coatings. In this model, R_s corresponds to the resistance of the solution, Rp the resistance of porous layer, R_b the resistance of barrier layer, Cp the capacitance of porous layer and Q_b the capacitance of barrier layer. A constant-phase element representing a shift from the ideal capacitor was used instead of the capacitance itself, for simplicity. The impedance of a phase element is defined as $Z_{CPE} = [Q(jw)^{\alpha}]^{-1}$, where $-1 \leq \alpha \leq 1$. The value of α is associated with the non-uniform distribution of current as a result of roughness and surface defects. The resistance and capacitance values of the porous and barrier layers are given in Table 1. According to the proposed model, the passive film consists of two layers, the inner barrier layer, whose resistance value, R_b, is significantly larger than the value associated to the outer porous layer, $R_{p,}$ as shown in Table 1. These results indicate that the protection provided by the passive layer is predominantly due to the inner layer. The porous oxide layer may becomes hydrated and ions forming RS solution especially chloride ions may be easily incorporated into the pores and subsequently precipitate, leading to either corrosion or self-healing. The resistance value increases with increasing of immersion time may be due to incorporation of Cl^- ions through defect sites and

formation of resistive transitory compounds in the film with time [6]. Also, hydroxyl (OH^-) and calcium ions can be adsorbed with time.

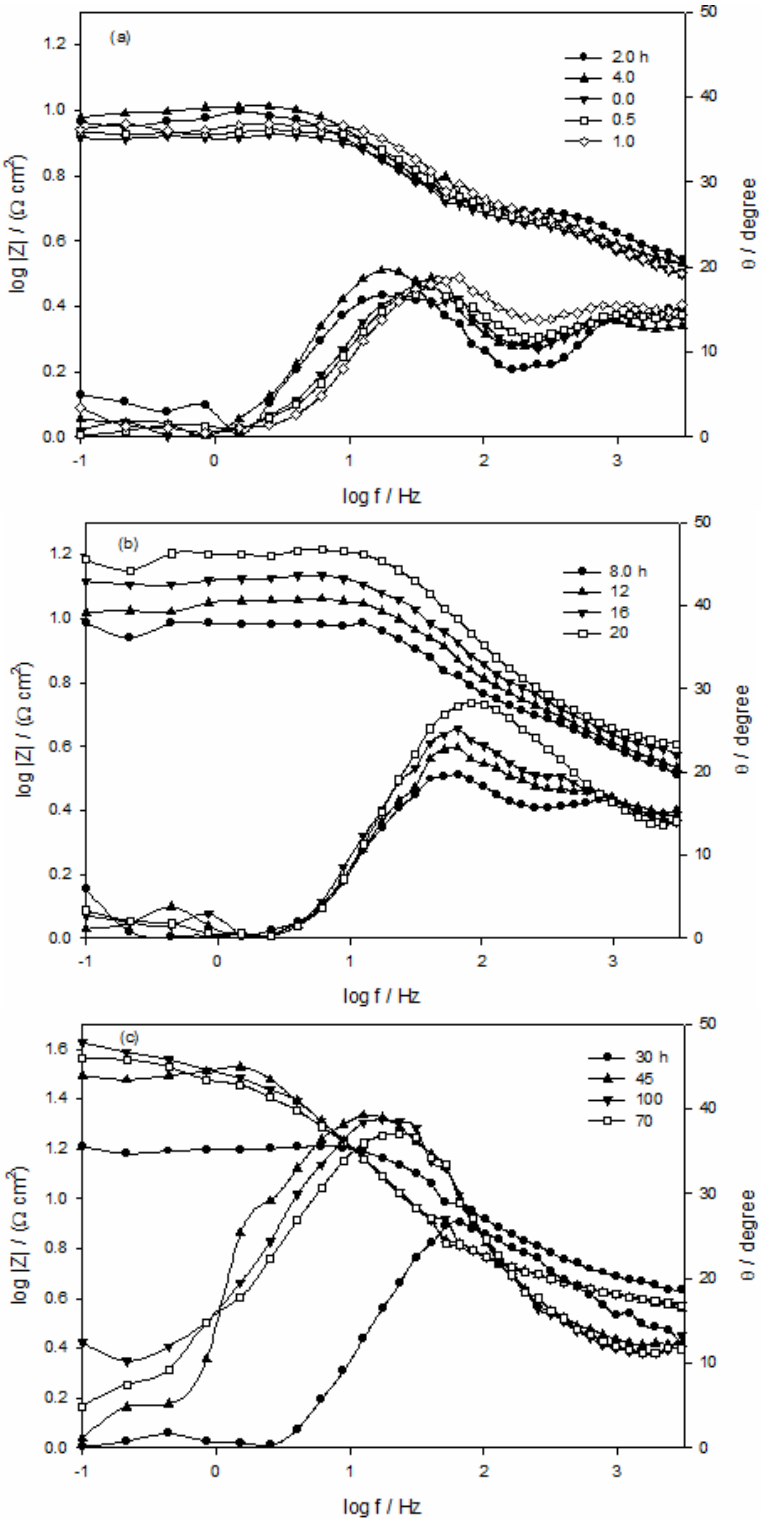

Figure 3 (a-c). Bode plots of AZ31E alloy as a function of immersion time in RS at 37 ^oC.

It was proved electrochemically that titanium alloys [1] have high resistances as a result of their very stable oxide films formed by titanium dioxide (TiO_2) and some suboxides TiO [1]. The physiological and electrochemical properties of the titanium dioxide film and its long-term stability in biofluids play an important role for the biocompatibility of titanium implant alloys [1]. These materials can release ions into the surrounding tissues and can produce certain reactions. Titanium, aluminum and vanadium ions can affect the cell function and inhibit the mineralization process at the bone-implant interface. Generally, titanium alloy is highly passive even at high chloride concentration containing media.

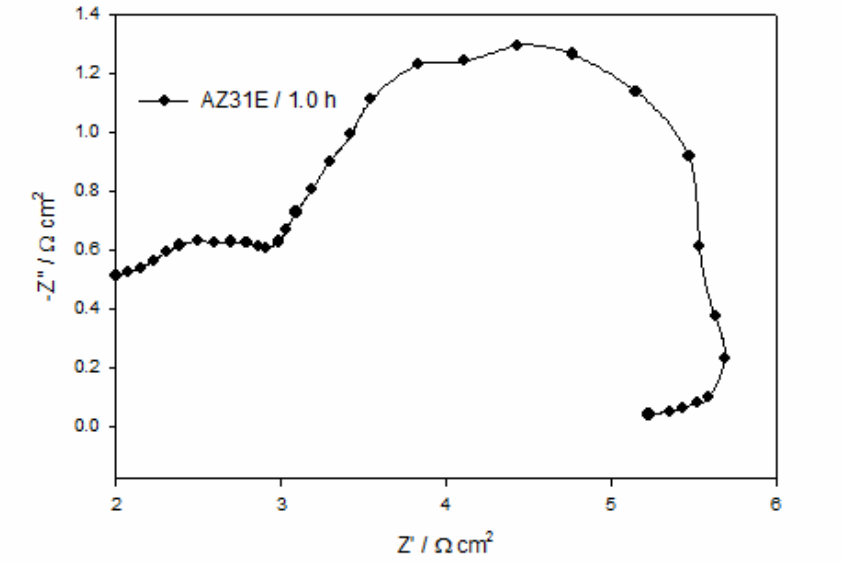

Figure 4. Nyquist plot after 1 h of immersion in RS at 37 ^{o}C.

The EIS scans as Bode plots, in Fig. 3a-c, for AZ31E alloy, as a function of immersion time, were recorded in the test solution for 100 h. The diagrams show resistive regions at high frequencies. The impedance (|Z|) as well as phase shift (θ) values of AZ31E alloy is clearly dependent on immersion time. It is of inertest to observe that an increase in the time of immersion, from 0 to 4.0 h (Fig. 3a), gradually increases the |Z| value, whereas θ_{max} is nearly constant. From 8.0 to 20 h (Fig. 3b), the impedance and θ_{max} values increase gradually. For larger immersion time from 30-70 h (Fig. 3c), both |Z| value and θ_{max} values increase sharply. The results in general show that Bode plots display two maximum phase lags. Fig. 4, as an example for 1h immersion of AZ31E alloy, manifested two depressed capacitive semicircles, typical of Randles element, at higher and lower frequencies regions, separated by an inductive loop at intermediate frequencies. Inductive loops can be explained by the occurrence of an adsorbed intermediate species on the surface. The experimental data were consistent with the involvement of the intermediate species Mg^+ in magnesium dissolution at film imperfections or on a film-free surface. At such sites, magnesium is first oxidised electrochemically to intermediate species Mg^+, then the intermediate species react chemically with water to produce hydrogen and Mg^{2+}. The presence of Cl^- ions increases the film free area, and accelerates the electrochemical reaction rate

from magnesium metal to Mg^+ [6]. The capacitive semicircle at higher frequencies is attributed to the redox Mg–Mg^+ reaction since it was assumed to be the rate determining step in the charge transfer process. Therefore, the resistance value obtained from intercepts of the first capacitive semicircle with real axis corresponds to the charge transfer resistance. On the other hand, the second capacitive semicircle could be attributed to the fast complementary corrosion reaction. The curve manifested that addition of chloride ions leads to an increase in the size of the capacitive semicircles with immersion time, indicating an increase in the resistance and a decrease in the corrosion rate. The increase in resistivity arises from the change in chemical composition of the surface film due to the incorporation of Cl^- ions into the film especially through defect sites with low ionic resistance.

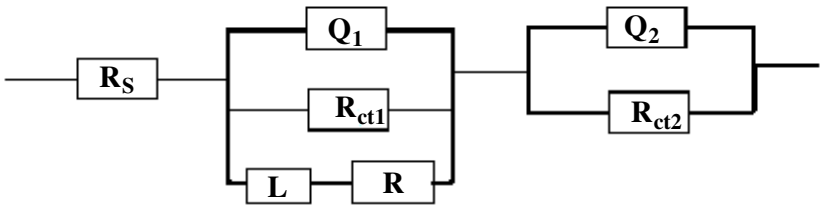

Figure 5. Equivalent circuit model representing two series time constants for an electrode/electrolyte solution interface.

The impedance data were thus simulated to the appropriate equivalent circuit for the case with two time constants (Fig. 5). The model includes the solution resistance R_s, a series combination of resistance, R, and inductance, L, in parallel with charge transfer resistance $(R_{ct})_1$, and the constant phase element (CPE_1). In the high frequency limit, the inductive contribution to the overall impedance is insignificant. Therefore, the Nyquist plot of the impedance is a semicircle characteristic of the parallel arrangement of the double layer capacitance and charge transfer resistance corresponding to the corrosion reaction. Contribution to the total impedance at intermediate frequencies comes mainly from the charge transfer resistance and inductive component in parallel. The inductor arising from adsorption effects could be defined as ($L = R\tau$), where τ is the relaxation time for adsorption on the electrode surface. The low frequency locus displays the characteristics of a parallel RC circuit. This circuit includes another constant phase element (CPE_2) which is placed in parallel to charge transfer resistance element $(R_{ct})_2$. The $(R_{ct})_2$ value is a measure of charge transfer resistance corresponding to the Mg^+–Mg^{2+} reaction. The CPE is used in this model to compensate for non-homogeneity in the system and is defined by two values, Q and α. The impedance of CPE is represented by $Z_{CPE} = Q^{-1}(i\omega)^{-\alpha}$, where $i = (-1)^{1/2}$, ω is frequency in rad s^{-1}, $\omega = 2\pi f$ and f is the frequency in Hz. If α equals one, the impedance of CPE is identical to that of a capacitor, $Zc = (i\omega C)^{-\alpha}$ and in this case Q gives a pure capacitance (C). For non-homogeneous systems, α value is in the range from 0.9–1. Computer fitting of the spectrum allows evolution of the elements of the circuit analogue. The aim of the fitting

procedure is to find the values which best describe the data. The experimental and computer fit results are given in Table 2. It was found that fit results were consistent with the experimental data within 5% error.

As shown in Table 2, film healing and thickening becomes effective by increasing the time of immersion in Ringer's solution, leading to a quasi-steady state thickness at longer times. This is caused by the formation of adherent corrosion products on the sample surface as $Mg(OH)_2$ which is precipitated from the solution during the corrosion of magnesium alloys due to saturation and localized alkalization [2] . This is confirmed by measuring the pH of Ringer's solution after completing the experiment, which becomes 11.0. Recently, Hassel et al. [7] reported that Ca could improve both the corrosion resistance in NaCl solution and mechanical properties of magnesium alloy. Moreover, Ca is a major component in human bone and can accelerate the bone growth [8,9]. It was thought that the presence of Ca ion benefits the bone healing. However, for chloride ions, low corrosion rates were obtained due to the formation of a partially protective $Mg(OH)_2$ layer and increases in hydrogen evolution. The growth of the polarization resistance with the immersion time is consistent with the continual decrease of the bio-corrosion rate.

Table 2. Impedance parameters of AZ31E alloy in RS at 37 ^{o}C.

Time	R_s /	$(R_{ct})_1$ /	Q_1 /	α_1	R /	L /	$(R_{ct})_2$ /	Q_2 /	α_2
hour	Ω cm^2	Ω cm^2	μF cm^{-2}		Ω cm^2	H	Ω cm^2	μF cm^{-2}	
0.00	0.18	5.29	416.9	0.98	53.45	0.032	5.40	154.3	0.94
0.50	0.18	5.31	311.2	0.98	54.90	0.035	5.67	90.05	0.94
1.00	0.18	5.32	299.3	0.96	56.27	0.040	5.89	89.13	0.95
2.00	0.18	5.32	172.1	0.97	60.49	0.044	6.01	86.79	0.97
4.00	0.18	5.33	161.9	0.97	67.35	0.051	6.29	81.07	0.96
8.00	0.19	5.35	157.7	0.99	73.36	0.055	7.34	72.45	0.93
12.00	0.19	5.37	147.6	0.99	86.83	0.059	8.37	69.95	0.95
16.00	0.19	5.38	146.9	0.98	105.2	0.061	9.01	55.87	0.94
20.00	0.19	5.38	143.8	0.99	106.2	0.061	9.06	45.21	0.98
30.00	0.22	6.37	139.8	0.99	248.3	0.145	24.9	41.14	0.97
45.00	0.39	6.40	135.5	0.98	258.7	0.147	25.1	30.30	0.97
70.00	0.58	6.45	132.8	0.99	307.5	0.151	30.6	17.15	0.97
100.00	0.59	6.53	116.3	0.99	405.1	0.154	36.8	14.23	0.98

Nevertheless, for any given time, the resistance of the film formed on Ti alloy shows always higher values compared to the values of Mg alloy, as given in Tables 1&2, respectively. This is due to the fact that the film formed on magnesium alloy is more porous than that formed on titanium alloy, which is thin and compact [5].

3.2. SEM measurements

For Ti-6Al-4V, (Fig. 6a) shows that mechanically polished titanium alloy surface is smooth before immersion (blank). After 100 h of immersion in RS, it is clear that the alloy surface is covered with a thin layer that corresponds to the passive film formed on it.

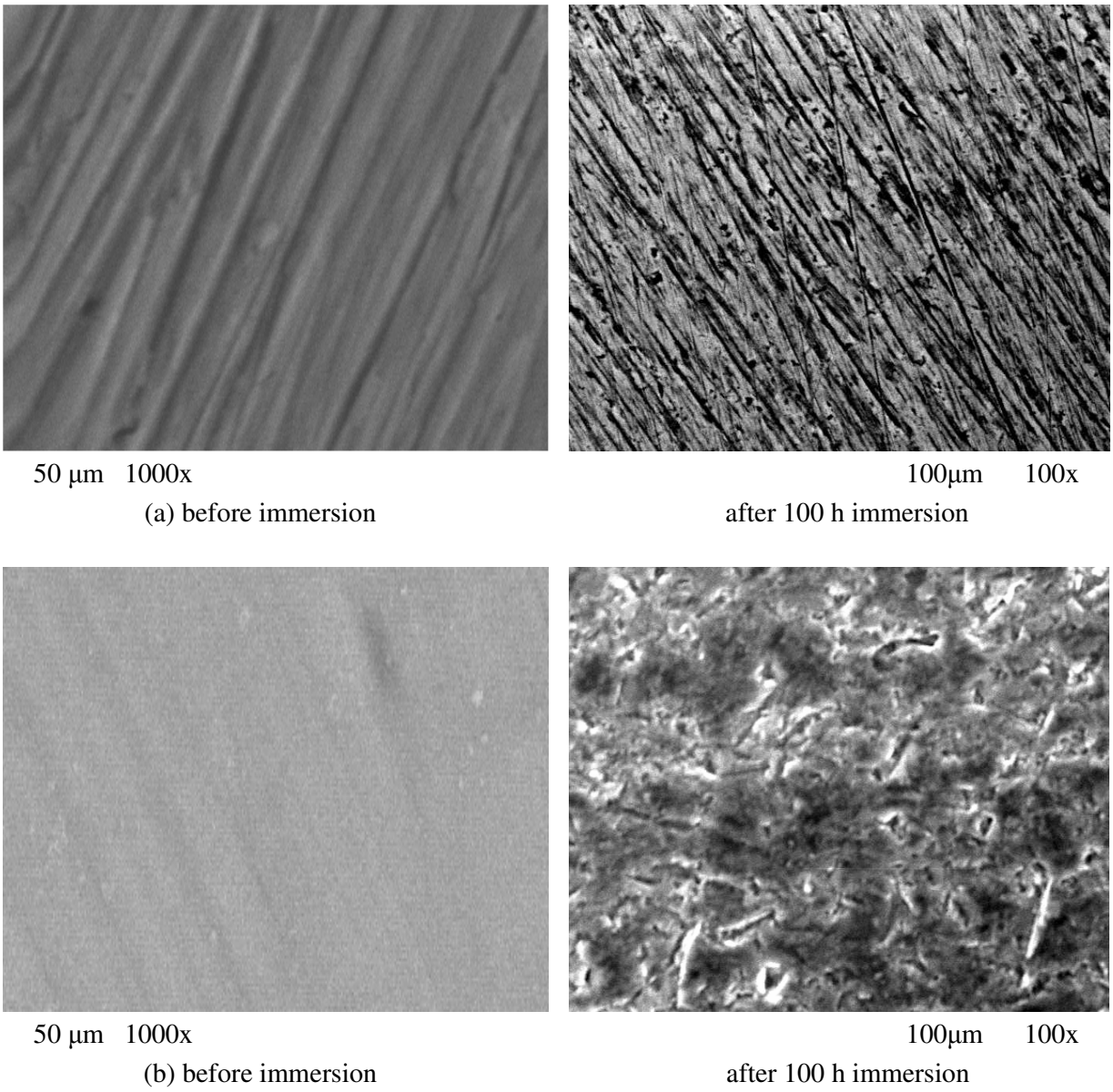

Figure 6. SEM images of (a) Ti-6Al-4V alloy and (b) AZ31E in air after polishing (blank) and in RS at 37 ^{o}C after 100 h of immersion.

SEM examination of AZ31E alloy surface after 100 h immersion in the same RS is shown in Fig. 6b, as compared to that of the uniform distribution for polished sample (blank). After immersion;

it shows microcracks [2], which indicate the existence of a vulnerable film. There are plenty of visible corrosion products on the surface of AZ31 after 100 h immersion.

3.3. Potentiodynamic polarization

Polarization behavior of Ti-6Al-4V was followed by scanning from -1.0 to -0.5 V and AZ31E alloy from -2.0 to -0.5 V, vs. SCE (Fig. 7) after 100 h of immersion using potentiodynamic polarization measurements at a scan rate of 1.0 mV s^{-1} in Ringer's solution.

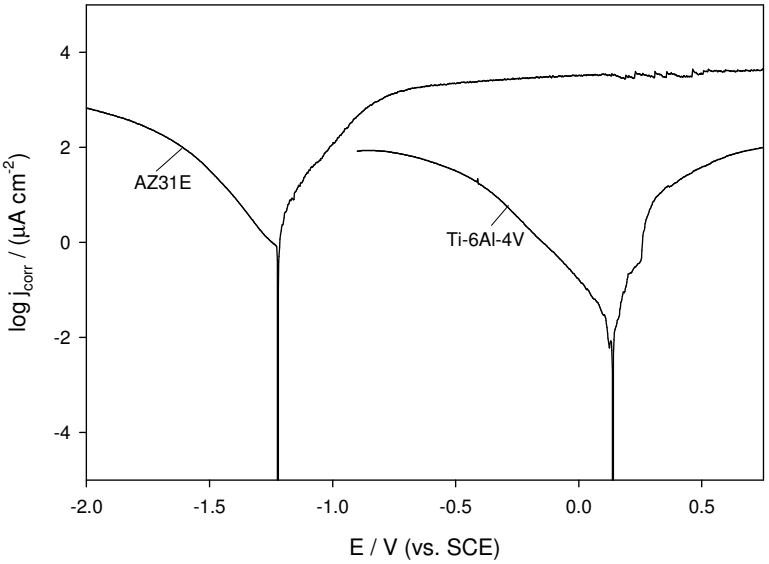

Figure 7. Potentiodynamic polarization curves of Ti-6Al-4V and AZ31E alloys in RS at 37 ^{o}C.

These results enable the determination of various electrochemical corrosion parameters of the two electrodes using Thales software for i/E analysis [10,11]. To avoid the presence of some degree of nonlinearity in the Tafel slope region of the obtained polarization curves, the Tafel constants were calculated as the slope of the points after E_{corr} by 50 mV, using a computer least squares analysis. The corrosion current was then determined by the intersection of the cathodic or the anodic Tafel line with the OCP (potential of zero current in the potentiodynamic curves or E_{corr}). This point determines the potential (E_{corr}) and current density (i_{corr}) for corrosion.

For all tested electrodes the active dissolution parameter values, corrosion potential (E_{corr}), corrosion current density (i_{corr}), Tafel slopes (β_a and β_c) were calculated and presented in Table 3. For Ti alloys, the first alloy registered as implant material in the ASTM standards was (F-136-84) [2]. The value of i_{corr} is much lower than that for magnesium alloy. Generally, titanium alloy is much more passive than magnesium alloy as implant material. However, it needs another surgery to be removed from the human body after the bone is healed. On the other hand, magnesium alloys (AZ31E alloy as biodegradable alloy) can be used in the human body for bone healing due to its higher corrosion

current density than titanium alloy. It is also of lower cost and lighter weight [12-14] than titanium alloy. Biodegradable implant materials as AZ31E alloy in the human body can be gradually dissolved, absorbed, consumed or excreted [15], so there is no need for second surgery to remove implants after surgery regions healed. There is growing evidence that if the releasing of Mg^{2+} is acceptable by human body, it will help to stimulate the healing of bone tissue.

Generally, in water solutions containing chloride ions, the passive $Mg(OH)_2$ layer is destroyed and dissolved. Formation of hydrogen is the main cathode reaction, the source of porous corrosion layer is the inhomogeneous crystal structures, e.g., when $Mg_{17}Al_{12}$ phase is precipitated on grain boundaries. These structures have higher standard potential and they cause electrolytic process within the surrounding matrix. This electrochemical corrosion creates traces of porous corrosion product. In the Mg alloys, the pressure corrosion cracking appears when the internal or external tensile stresses are combined with the effect of corrosion media (chloride solutions). This leads to brittleness at the crack points because hydrogen, formed during the corrosion process, is absorbed [16].

After the dissolution of the hydroxide film, the primary anodic reaction (the dissolution of magnesium) occurs:

$$Mg \rightarrow Mg^{2+} + 2e^- \quad (1)$$

Spontaneously, the cathodic reaction (the reduction of protons) occurs:

$$2H_2O + 2e^- \rightarrow 2OH^- + H_2\uparrow \quad (2)$$

The OH^- produced in reaction (2) leads to the pH increase at the corrosion interface. Once the interfacial pH is high enough, Mg^{2+} will precipitate as solid hydroxide $Mg(OH)_2$ (The solubility product constant p*K*sp of Mg $(OH)_2$ is 11.25 [17] and then deposit on the alloy surface as following [18]:

$$Mg^{2+} + 2OH^- \rightarrow Mg(OH)_2 \text{ (product formation)} \quad (3)$$

The unsolvable corrosion product $Mg(OH)_2$ precipitates on the surface of magnesium alloy and form a surface layer. The layer could protect the magnesium alloy from being corroded slightly. However, this protection effect is very poor because that the $Mg(OH)_2$ layer is not compact [18]. When corrosive medium containing Cl^- contacts with AZ31 magnesium alloy, Cl^-, a kind of aggressive ion with small radius, can penetrate this loose $Mg(OH)_2$ layer easily, reach the surface of the magnesium alloy and accelerate the reaction (1). Therefore, the surface layer which composed with the corrosion products $Mg(OH)_2$ only has a little protective function for the magnesium alloys in the solution with Cl^-, which led to that the current increased sharply upon the anodic overpotential increasing as if the $Mg(OH)_2$ layer did not exist.

Thus, AZ31E alloy is much more corroded than titanium alloy in Ringer's solution, however, magnesium alloy is preferred in human body because of no need to second surgery for removing it and its low cost.

4. CONCLUSIONS

- Corrosion resistance for Ti–6Al–4V or AZ31E in RS increases with increasing immersion time.
- For any given time, the resistance of the film formed on Ti alloy has always a higher value as compared to the value of AZ31E alloy.
- Polarization results show that titanium alloy is much more passive than magnesium alloy as indicated by its low corrosion current density and hydrogen evolution rate compared to that of magnesium alloy.
- Thus magnesium alloy is much better to be used in human body due to it is as biodegradable implant material can be gradually dissolved, absorbed, consumed or excreted from human body. So there is no need for second surgery to remove implants after surgery regions healed as in case of titanium.

References

1. V. Popa, I. Demetrescu, S.H. Suh, E. Vasilescu, P. Drob, D. Ionita, C. Vasilescu, *Bioelectrochemistry* 2007; 71:126–134
2. A.M. Fekry, R.M. El-Sherief, *Electrochim. Acta* 54 (2009) 7280-7285.
3. M.P. Staiger, A.M. Pietak, J. Huadmai, G. Dias, *Biomaterials* 27 (2006) 1728–1734.
4. M.R. Souto, M.M. Laz, R.L. Reis, *Biomaterials* 24 (2003) 4213-4221.
5. I.C. Lavos-Valereto, S. Wolynec, I. Ramires, A.C. Guastaldi, I. Costa , *J. Mater. Sci. Mater. Med.* 15 (2004) 55-59.
6. G. Song, A. Atrens, S. St John, X. Wu, J. Nairn, *Corros. Sci.* 39 (1997) 1981-2004.
7. T. Hassel, F.W. Bach, A. Golovko, C. Krause, Magnesium technology in the global age, in: 45th Annual Conference of Metallurgists of CIM, Montreal, Quebec, Canada, (2006) 359–370
8. J.Z. Ilich, J.E. Kerstetter**,** *J. Am. Coll. Nutr***.** 19 (2000) 715–737.
9. C.M. Serre, M. Papillard, P. Chavassieux, J.C. Voegel, G. Boivin, *J. Biomed. Mater. Res*. 42 (1998) 626–633.
10. A.M. Fekry, *Electrochim. Acta* 54 (2009) 3480-3489.
11. M.A. Ameer, A.M. Fekry, A.A.Ghoneim, F.A.Attaby, *Int. J. Electrochem. Sci.* 5 (2010) 1847 – 1861.
12. F.E. Heakal, A.M. Fekry, M.Z. Fatayerji, *Electrochim. Acta* 54 (2009) 1545–1557.
13. A.M. Fekry , *Int. J. Hydrogen Energy* 35 (2010) 12945-12951.
14. A.M. Fekry, M.Z. Fatayerji, *Electrochim. Acta* 54 (2009) 6522–6528.
15. A.A. Ghoneim, A.M. Fekry, M.A. Ameer, *Electrochim. Acta* 55 (2010) 6028–6035.
16. L.I. Lingjie, L.E.I. Jinglei, P.A.N. Fusheng, Magnesium Alloys-Corrosion and Surface Treatments, Frank Czerwinski (Ed.), ISBN: 978-953-307-972-1, InTech, (2010) Ch3:29.
17. J. Dean, Lange's handbook of chemistry (15th Ed.), McGraw-Hill, Inc., ISBN 0-07-016384-7, New York, (1999)
18. G. Song, The corrosion and protection of magnesium alloys, Chemical Industry Press of China, ISBN 7-5025-8565-6, Beijing, (2006)